Numerical investigation on properties of attack angle for an opposing jet thermal protection system*

Lu Hai-Bo(陆海波)† and Liu Wei-Qiang(刘伟强)

Science and Technology on Scramjet Laboratory, National University of Defense Technology, Changsha 410073, *China*

(Received 8 January 2012; revised manuscript received 14 February 2012)

The three-dimensional Navier–Stokes equation and the k–ε viscous model are used to simulate the attack angle characteristics of a hemisphere nose-tip with an opposing jet thermal protection system in supersonic flow conditions. The numerical method is validated by the relevant experiment. The flow field parameters, aerodynamic forces, and surface heat flux distributions for attack angles of 0°, 2°, 5°, 7°, and 10° are obtained. The detailed numerical results show that the cruise attack angle has a great influence on the flow field parameters, aerodynamic force, and surface heat flux distribution of the supersonic vehicle nose-tip with an opposing jet thermal protection system. When the attack angle reaches 10°, the heat flux on the windward generatrix is close to the maximal heat flux on the wall surface of the nose-tip without thermal protection system, thus the thermal protection has failed.

Keywords: properties of attack angle, opposing jet, thermal protection system, supersonic vehicle, computer simulation

PACS: 44.05.+e, 47.40.ki **DOI:** 10.1088/1674-1056/21/8/084401

1. Introduction

In the development of high speed vehicles, one of the most important problems is the severe aerodynamic heating at the nose of the vehicle during supersonic and re-entry flight. Thermal analysis and control are always the central topics of research in thermal fields[1−3] and much attention is always paid to the design of the thermal protection system (TPS) of high speed vehicles.[4−6]

Generally, the methods of designing the TPS of high speed vehicles are divided into two kinds. One is passive method and the other is active method. The passive method is to protect the body from heating by using heat protection materials and ablators. The active method is to protect the body surface by using injection gases or mechanical devices.

The opposing jet is a kind of effective TPS for supersonic and re-entry vehicles. In the early 1960s, the opposing jet was reported as an efficient thermal protection technique for the nose-tip of hypersonic vehicles, and validating experiments were conducted.[7] More studies on the opposing jet flow have been conducted in the 21st century. Aerodynamic heating reduction due to an opposing jet from the top of blunt body was investigated experimentally and numerically by Aso *et al.*,[8] and it has been proved to be quite effective at the nose of the blunt body. Detailed numerical investigation of the flow field indicates that the recirculation region plays an important role in reducing aerodynamic heating. The effect of the ratio of total pressure of opposing jet to free stream on the reduction of aerodynamic heating was investigated by Hayashi *et al.*[9,10] The experimental and numerical results show that as the pressure ratio increases, the heat flux decreases at each point of the nose surface. The detailed influences of the free stream Mach number, jet Mach number, and angle of attack on the reduction of drag coefficient were studied by highly accurate simulation of the Navier–Stokes equations in Ref. [11].

As shown in Fig. 1, for an opposing jet TPS, the jet flow acts as a mechanical spike. It detaches the free stream from the body surface and the coolant gas forms the recirculation region, then the hot free stream cannot reach the body surface directly. So, the aerodynamic heating is reduced.

The vehicle flight with attack angle is inevitable, the cruise attack angle of high speed vehicle are commonly between ±10°.[12] With a big angle of attack,

*Project supported by the National Natural Science Foundation of China (Grant No. 90916018), the Research Fund for the Doctoral Program of Higher Education of China (Grant No. 200899980006), and the Natural Science Foundation of Hunan Province, China (Grant No. 09JJ3109).

†Corresponding author. E-mail: lhbboo@sohu.com

© 2012 Chinese Physical Society and IOP Publishing Ltd

there should be an obvious influence on the "air spike", but less research has been conducted on it. In the present study, we just concentrate on this influence of the angle of attack. The numerical method is validated by the available experimental data in the published literature. Due to the angle of attack, remarkable variations of the flow field parameters, aerodynamic force and surface heat flux distribution are revealed by detailed numerical simulation.

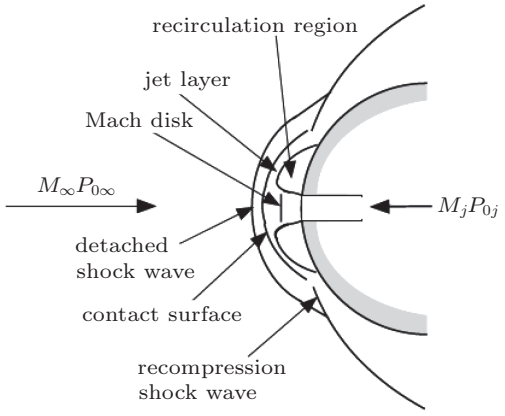


Fig. 1. Flow field of the opposing jet to the supersonic main stream.[10]

2. Numerical method

2.1. Governing equation and discretization

The three-dimensional (3D) Navier–Stokes equation is given by

$$\frac{\partial U}{\partial t}+\frac{\partial E}{\partial x}+\frac{\partial F}{\partial y}+\frac{\partial G}{\partial z}=\frac{\partial E_v}{\partial x}+\frac{\partial F_v}{\partial y}+\frac{\partial G_v}{\partial z}, \quad (1)$$

where U is the conservation variable, E, F, and G are the inviscid terms, E_v, F_v, and G_v are the viscous terms. Equation (1), solved with the k–ε turbulence model,[13] is used as a governing equation.

The convective terms are approximated using the AUSM-DV splitting method,[14] where a MUSCL approach with Min-mod limiter is implemented to increase the numerical accuracy, and the central difference method is used for the viscous terms. The LU-SSOR scheme is used for the time integration.

2.2. Generation of grids

The nose-tip model is a hemispherical one with a diameter of 50 mm and the nozzle exit of the opposing jet is located at the stagnation point with a diameter of 4 mm. The three-dimensional (3D) boundary-fitted grids for the nose-tip with the TPS are generated by the Poisson equations[15]

$$\begin{cases} \nabla^2_{(x,y,z)}\xi = P, \\ \nabla^2_{(x,y,z)}\eta = Q, \\ \nabla^2_{(x,y,z)}\varsigma = R, \end{cases} \quad (2)$$

where (x, y, z) are the coordinates of the physical space, (ξ, η, ς) are the coordinates of the calculation space, and P, Q, R are the source item which regulate the refinement of the grid.[16,17] The grids of the model in the symmetrical plane, outlet, and the wall of the nose-tip are shown in Fig. 2.

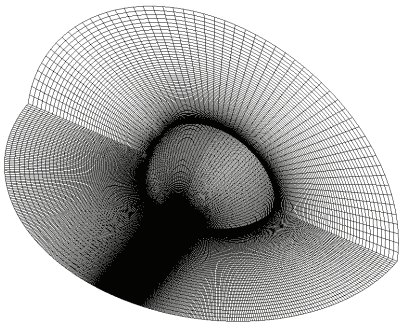


Fig. 2. Grid of the simulation model.

2.3. Boundary conditions and numerical assumption

The boundary conditions are shown in Table 1. The wall boundary condition is assumed to be no-slip and isothermal (the wall temperature $T_{\rm w} = 295$ K).

Table 1. Boundary conditions.

Free stream			Opposing jet flow		
Symbol	Quantity	Value	Symbol	Quantity	Value
$Ma_{\rm free}$	Mach number	3.98	$Ma_{\rm opp}$	Mach number	1.0
P_0/MPa	total pressure	1.37	PR	ratio of total pressure of free stream to opposing jet	0.4
$T_{0-{\rm free}}$/K	total temperature	397	$T_{0-{\rm opp}}$/K	total temperature	300

3. Code validation

The Stanton number based on the free stream condition is given by the following expression:

$$St = \frac{q_{\rm w}}{(T_{\rm aw} - T_{\rm w}\rho_\infty c_{p\infty} u_\infty}, \tag{3}$$

$$T_{\rm aw} = T_\infty\{1 + \sqrt[3]{Pr}[(\gamma - 1)/2]M_\infty^2\}, \tag{4}$$

where $q_{\rm w}$ is the heat flux, $T_{\rm aw}$ is the temperature of the thermal isolation wall, $T_{\rm w}$ is the temperature of the outer body surface, ρ_∞ is the density of the free stream, $c_{p\infty}$ is the constant-pressure specific heat of the free stream, u_∞ is the velocity of the free stream, Pr is Prandtl number, γ is the specific heat ratio, and M_∞ is the Mach number of the free stream.

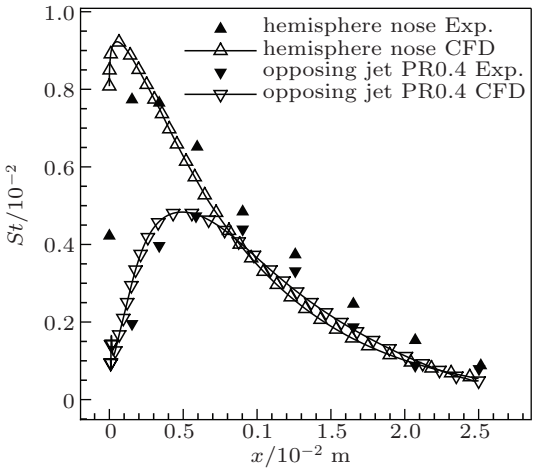


Fig. 3. Stanton number comparison.

The predicted Stanton numbers along the surface of the traditional hemisphere nose (without an opposing jet) and the nose with the opposing jet are compared with the experimental data[10] as shown in Fig. 3, showing numerical and experimental results are in good agreement with each other. For the predicted St of the nose with the opposing jet, there are eight experimental data points, except the first one, the simulation accuracies of the remaining points are in 15%, of which the best one is close to 0.9%. The discrepancy is attributed to the assumption of the simulation model, computation error and experimental measurement error, especially in the vicinity of the peak of the nose where the flow is more complicated.

4. Results and discussion

4.1. Flow Field

The distributions of the streamlines (Ma contours), temperature, and pressure of the nose-tip with attack angle 0° are shown in Fig. 4. From Fig. 4, it is evident that a Mach disk is formed in order to balance the pressure of the opposing jet and the pressure downstream the detached shock wave. The opposing jet meets the free stream and forms the interface. The free steam lets the jet layer reattach to the body surface, and a recirculation region is formed. The recompression shock wave is formed downstream the reattachment of the jet layer. A typical flow field of opposing jet to supersonic main stream like Fig. 1 is obtained by the simulation.

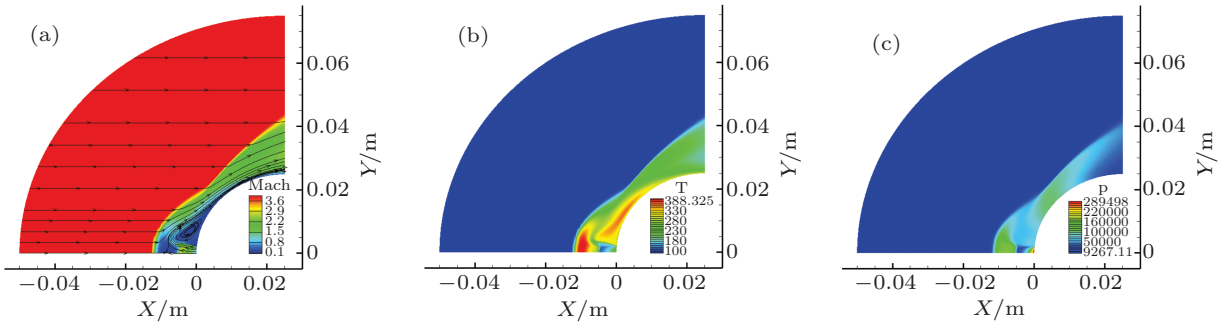


Fig. 4. (colour online) Flow field of opposing jet TPS nose with attack angle 0°, (a) streamline (Ma contours), (b) temperature, (c) pressure.

The distributions of the streamlines (Ma contours) of the nose-tip with variable attack angles of 2°, 5°, 7°, and 10° are shown, respectively, in Fig. 5. It is obvious that the recirculation region beside the windward generatrix is pushed upward by the free stream with the angle of attack and the recirculation region beside the leeward generatrix is dragged to the backside. This phenomenon becomes more evident with the increase of angle of attack. The Mach disk and the jet layer distribute in up–down symmetry with small angle of attack. But in the angle of attack 10° condition, the distributions of the Mach disk and the jet layer are tilted.

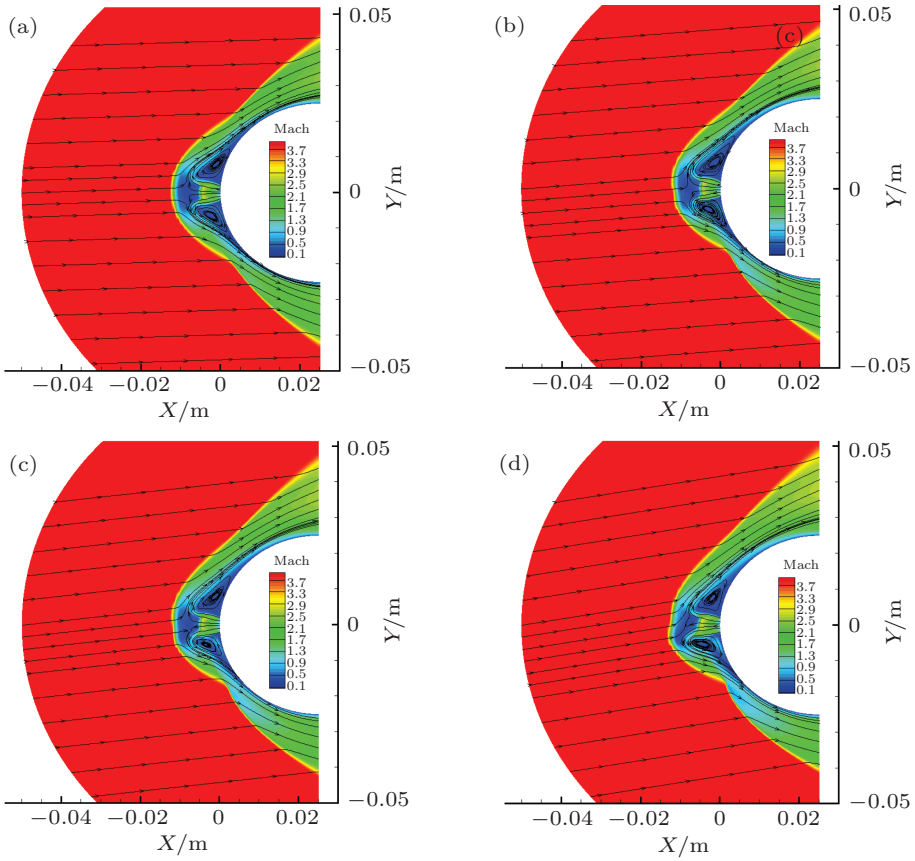


Fig. 5. (colour online) Streamlines (contours of Ma) of opposing jet TPS nose with variable attack angle in symmetrical plane, (a) attack angle 2°, (b) attack angle 5°, (c) attack angle 7°, (d) attack angle 10°.

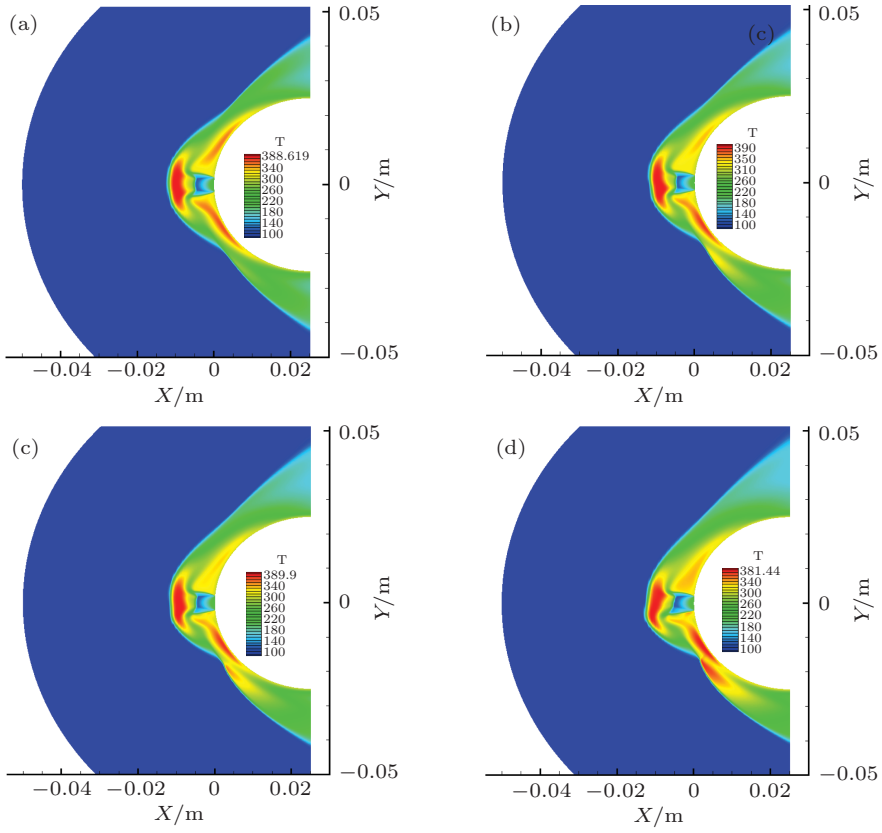


Fig. 6. (colour online) Temperature distribution of opposing jet TPS nose with variable attack angle in symmetrical plane: (a) attack angle 2°, (b) attack angle 5°, (c) attack angle 7°, and (d) attack angle 10°.

The distributions of the temperature and pressure of the nose-tip with variable attack angles of 2°, 5°, 7°, and 10° are shown in Figs. 6 and 7, respectively. As shown in the figures, with the increase of the angle of attack, the recompression shock wave on leeward generatrix becomes weaker and finally combines with the detached shock wave. On the windward generatrix, the recompression shock wave becomes stronger, an extra high temperature and high pressure region is formed behind the recompression shock wave. And there is a local high temperature region formed under the exit of the opposing jet in front of the nose-tip surface.

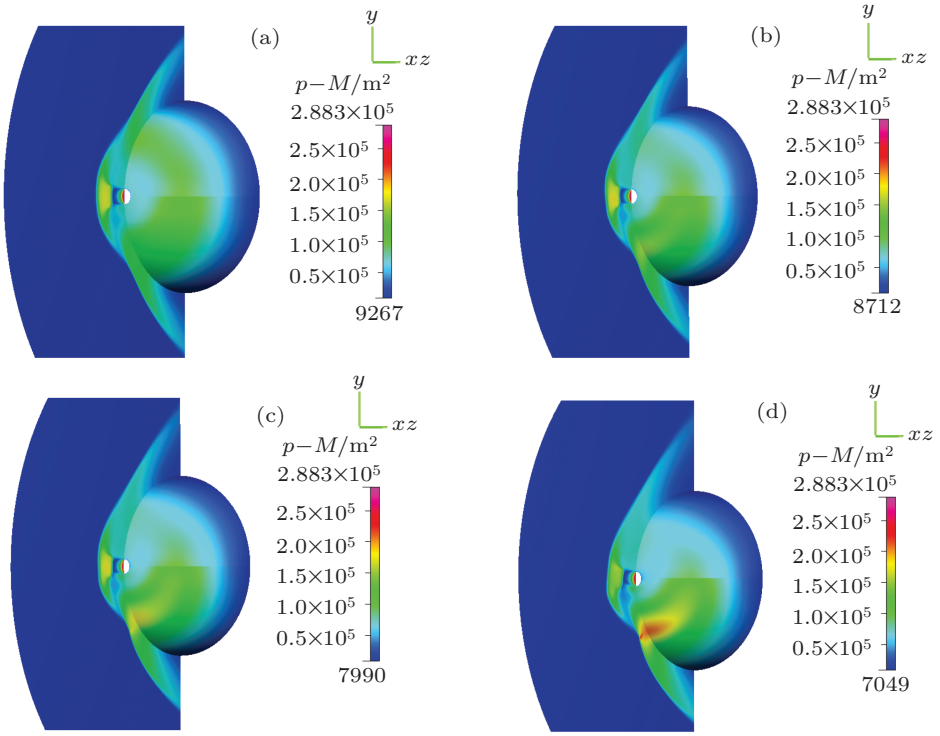


Fig. 7. (colour online) Pressure distribution of the opposing jet TPS nose with variable attack angle in symmetrical plane and nose surface: (a) attack angle 2°, (b) attack angle 5°, (c) attack angle 7°, (d) attack angle 10°.

4.2. Aerodynamic force

The drag coefficient (Cd), lift coefficient (Cl), and lift–drag ratio (L/D) of the opposing jet nose with different angles of attack are shown in Table 2. The referenced area is the bottom surface of the nose-tip (diameter 50 mm). Between 0° and 5°, the Cd increases with the increase of the angle of attack. However, from 5° to 10°, the drag coefficient (Cd) does not increase monotonically with the increase of the attack angle, and the variation of the Cd is small. As shown in Figs. 4–7, with the increase of the attack angle, the "air spike" formed by the opposing jet flow is affected by the free stream just like a mechanical one. So, there is an obvious increase of the lift coefficient (Cl) with the increase of the attack angle. The lift–drag ratio increases, too.

Table 2. Drag coefficient (Cd), lift coefficient (Cl), and lift–drag ratio (L/D).

Quantity	Value				
Angle of attack	0°	2°	5°	7°	10°
Cd	0.7486	0.7523	0.7704	0.7780	0.7765
Cl	0	0.05389	0.1312	0.1743	0.2348
L/D	0	0.07163	0.1703	0.2240	0.3020

4.3. Distribution of heat flux

The Stanton number distributions along the windward (down) and leeward (up) generatrix of the opposing jet nose-tip are shown in Fig. 8. The heat flux along the windward generatrix of the nose-tip is higher than that along the leeward generatrix by the influence of the attack angle. The heat flux along the windward generatrix of the nose-tip increases with the increase of the attack angle, but along the windward generatrix, it decreases. The maximum Stanton number along the windward generatrix of the nose-tip with 10° angle of attack is close to the peak value of the nose-tip without opposing jet. It can be considered that in this cruise angle of attack condition, the cooling efficiency of opposing jet TPS is too weak, so that the use of opposing jet TPS is unsuitable. Because of the local high temperature region which forms under the exit of the opposing jet in front of the nose-tip surface, there is a skip in the heat flux distribution of windward generatrix near the exit of the opposing jet. The larger the angle of attack, the more severe the skip is.

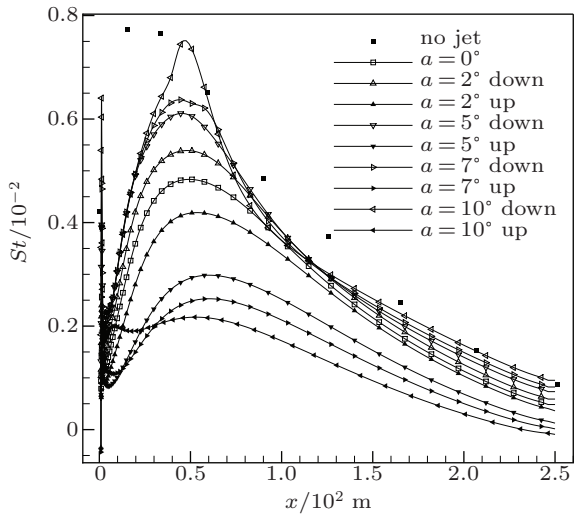


Fig. 8. Stanton number distributions.

5. Conclusion

Properties of attack angle for a hemispherical nose-tip with an opposing jet TPS of a supersonic vehicle are simulated numerically. The influence of the variable attack angle is discussed.

(i) The flow field of the opposing jet is tilted because of the cruise angle of attack. Both temperature and pressure in the windward surface are higher than those in the leeward surface.

(ii) In the condition of a smaller angle of attack (0°–5°), the drag coefficient (Cd) of the nose-tip with the opposing jet TPS increases with the increase of the angle of attack. In the condition of a larger angle of attack (5°–10°), there is little influence of angle of attack on the drag coefficient.

(iii) The lift coefficient (Cl) and lift–drag ratio (L/D) of the nose-tip increase with the increase of the attack angle.

(iv) The heat flux along the windward generatrix of the nose-tip is higher than that along the leeward generatrix one. With the increase of the attack angle, the heat flux increases along the windward generatrix increases, but decreases along the windward generatrix.

(v) The maximum Stanton number along the windward generatrix of the nose-tip with 10° angle of attack is close to the peak value of the nose-tip without TPS. It could be considered that in the condition of the free stream in this paper, the cooling efficiency of the opposing jet TPS is too weak or the use of an opposing jet TPS is unsuitable when the cruise angle of attack reaches 10°.

References

[1] Zhang Y, Zheng L C and Zhang X X 2009 *Acta Phys. Sin.* **58** 5501 (in Chinese)

[2] Zheng K C, Wen Z, Wang Z S, Lou G F, Liu X L and Wu W F 2012 *Acta Phys. Sin.* **61** 014401 (in Chinese)

[3] Huang C L, Feng Y H, Zhang X X, Wang G and Li J 2011 *Acta Phys. Sin.* **60** 114401 (in Chinese)

[4] Clay C L 2004 *J. Aircraft* **41** 978

[5] Glass D E, Merski N R and Glass C E 2002 *NASA/TM*-**2002**-211752

[6] Yang Y Z, Yang J L and Fang D N 2008 *Appl. Math. Mech.* **29** 47 (in Chinese)

[7] Warren C H E 1960 *J. Fluid Mech.* **8** 400

[8] Aso S, Hayashi K and Mizoguchi M 2002 *AIAA* **2002**-0646

[9] Hayashi K and Aso S 2003 *AIAA* **2003**-4041

[10] Hayashi K, Aso S and Tani Y 2005 *AIAA* **2005**-188

[11] Tian T and Yan C 2008 *J. Beijing Univ. Aeronaut. Astronaut.* **34** 9 (in Chinese)

[12] Hang W and Wang Z G 2008 *J. Solid Rocket Tech.* **31** 561 (in Chinese)

[13] Tao W Q 2001 *Numerical Heat Transfer* 2nd edn. (Xi'an: Xi'an Jiaotong University Press) (in Chinese)

[14] Azevedo J L F and Heidi K 1998 *AIAA* **1998**-2629

[15] Baker A J 1980 *NASA* CP-2166

[16] Middelcoff J F and Thomas P D 1979 *AIAA* **1979**-1462

[17] Chang K S and Choi C J 1986 *Int. Comn. Heat Mass Transfer* **13** 201